Heat Transfer Analysis for a Winged Reentry Flight Test Bed

Antonio Viviani antonio.viviani@unina2.it
Dipartimento di Ingegneria Aerospaziale e Meccanica (DIAM)
Seconda Università di Napoli (SUN)
via Roma 29, I-81031 Aversa, Italy

Giuseppe Pezzella g.pezzella@cira.it
Centro Italiano Ricerche Aerospaziali (CIRA)
via Maiorise, I-81043 Capua, Italy

Abstract

In this paper we deal with the aero-heating analysis of a reentry flight demonstrator helpful to the research activities for the design and development of a possible winged Reusable Launch Vehicle. In fact, to reduce risks in the development of next generation reusable launch vehicles, as first step it is suitable to gain deep design knowledge by means of extensive numerical computations, in particular for the aero-thermal environment the vehicle has to withstand during reentry. The demonstrator under study is a reentry space glider, to be used both as Crew Rescue Vehicle and Crew Transfer Vehicle for the International Space Station. It is designed to have large atmospheric manoeuvring capability, to test the whole path from the orbit down to subsonic speeds and then to the landing on a conventional runway. Several analysis tools are integrated in the framework of the vehicle aerothermal design. Between the others, we used computational analyses to simulate aerothermodynamic flowfield around the spacecraft and heat flux distributions over the vehicle surfaces for the assessment of the vehicle Thermal Protection System design. Heat flux distributions, provided for equilibrium conditions of radiation at wall and thermal shield emissivity equal to 0.85, highlight that the vehicle thermal shield has to withstand with about 1500 [kW/m^2] and 400 [kW/m^2] at nose and wing leading edge, respectively. Therefore, the fast developing new generation of thermal protection materials, such as Ultra High Temperature Ceramics, are available candidate to built the thermal shield in the most solicited vehicle parts. On the other hand, away from spacecraft leading edges, due to the low angle of attack profile followed by the vehicle during descent, the heat flux is close to values attainable with conventional heat shield. Also, the paper shows that the flying test bed is able to validate hypersonic aerothermodynamic design database and passenger experiments, including thermal shield and hot structures, giving confidence that a full-scale development can successfully proceed.

Keywords: Atmospheric Reentry, Nonequilibirum Hypersonic Flow, Aerothermochemistry, Aeroheating, Thermal Protection System, Ultra High Temperature Ceramics.

Nomenclature

D	Aerodynamic Drag, N
h	Specific enthalpy, J/kg
$\vec{J}$	Mass diffusion flux vector, kg/m^{2}s
k	Gas thermal conductivity, W/mK
Kn	Knudsen number
L	Aerodynamic Lift, N
M	Molar mass, kg/kgmole

$\hat{n}$	Unit normal
$\dot{q}$	Heat flux, W/m^2
Q	Integrated heat load, J/m^2
$\vec{r}$	Position vector, m
R	Radius, m
$\Re$	Universal gas constant, J/kgmole K
Re	Reynolds number
S	Surface, m^2
t	Time, s
T	Temperature, K
v	Flight-path speed, m/s

Greek Symbols

α	Angle of attack, deg
γ	Recombination coefficient
ρ	Density, kg/m^3
σ	Stefan-Boltzmann constant, W/m^{2}K

Subscripts

fm	Free molecular
FP	Flat Plate
LE	Leading edge
N	Nose
r	Reference value
s	Species
w	Wall
∞	Freestream conditions
0	Total (reservoir) conditions

1. INTRODUCTION

The need for a safer access to space dictates the review of operational capabilities and hence of design approach for manned reentry vehicles of next generation [1–3]. Up to now several hypersonic shapes have been investigated for use in recoverable space systems. Initial efforts focused on low Lift-to-Drag ratio (L/D), as Apollo spacecraft. Current systems such as the Space Shuttle, still fly at relatively low L/D (<1.5) but are reusable. Research has shown that reentry vehicle designs with high L/D could be designed to take advantage of aerodynamic lift during reentry. Higher L/D is desirable because it increases the area from which a re-entering vehicle can be recovered (e.g. reentry window) [4]. In fact, the times and locations from which the Space Shuttle can return are limited by its down-range and cross-range capability after reentry. A vehicle with high aerodynamic efficiency would have enhanced down-range and cross-range capability (more than twice that of the Space Shuttle). This leads to increase significantly the operational flexibility of reentry space launcher, for which the ability to reach demanding orbits and to return quickly for reuse will be critical to their operations and economics.

This paper presents results of the thermal protection analysis and design of a vehicle designed to serve as flying test bed in the framework of a reusable Two-Stage-To-Orbit (TSTO) space launch system development.

Considerable technological progress and strong multidisciplinary design optimization (MDO) approach, validated by in flight operations, are needed. Up to now, however, no practical experience exists in development and operation of a Reusable Launch Vehicle (RLV) in Europe, even if many candidate concepts for a future RLV have been proposed.

Although considerable progress has been achieved in hypersonics flow computations, and large wind tunnels exist, e.g. the “Scirocco” PWT (Plasma Wind Tunnel) at CIRA, this is by far not sufficient for the design of an operational space vehicle. For example, none of the upper atmosphere and hypersonic regime conditions have been explored in Europe for a winged vehicle. Further, space launch systems are still regarded as both costly and unsafe. To avoid substantial risks in developing a next generation RLV, it seems advisable to gain first a practical RLV design knowledge by in-flight demonstrations of scaled low cost prototype vehicle. To this end, we have integrated several analysis tools in the conceptual design process of a sharp edge Reentry Test Bed (RTB) able to perform a return to Earth.

RTB is a reentry space glider, with large atmospheric manoeuvring capability, expected to test the complete path from the orbit down to subsonic speeds and then landing on a conventional runway. Thus, it

will be able to validate hypersonic aerothermodynamic design database and passenger experiments, including Thermal Protection System (TPS) and hot structures.

The flight test bed, named VIPER-G1, is a prototype winged vehicle, embodying the critical technologies and the features of an operational system, giving confidence that a full-scale development can successfully proceed, with particular attention both on Crew Rescue Vehicle (CRV) and Crew Transfer Vehicle (CTV) development for the International Space Station (ISS).

The vehicle detailed design, however, is beyond the scope of this work and the mission and system requirements will be defined only at the level able to prove the concept feasibility. The overall goal is to perform a return back to Earth in a gentle winged descent (lifting return), involving both angle of attack (AoA) and bank angle modulation, keeping constant the temperature of the nose stagnation in the radiation equilibrium conditions (i.e. radiative cooling), restricting the g peak experienced to less than a tenth above normal ground-level values and, finally, with a wider than usual "reentry window" that would permit landing at any one of the many choices of airfields [5].

With a high cross range the vehicle can more easily meet the requirements for the return of an injured or sick crew member to an approved trauma center within few hours. Increasing a hypersonic vehicle L/D ratio, effectively increases the footprint in which the vehicle can safely maneuver and land. With an increased footprint, the vehicle can account for unforeseen reentry anomalies or for weather constraints at the prime landing sites and change course to an available site.

The key technologies, we have selected, include:

- low wing loading;
- high lift;
- sharp leading edges;
- advanced thermal protection system;

The assessment of the vehicle aeroheating environment is reported in the next paragraphs.

2. VEHICLE CONCEPT OVERVIEW

The vehicle concept consists of the following main elements: main body with a sharp nose, low aspect ratio wing, vertical stabilizer, wing and body flaps.

Several subsystems are necessary for the RTB flight: the Reaction Control System (RCS) to control the attitude of the demonstrator when the aerodynamic control surfaces are ineffective; the landing parachute, the avionics, electrics, and hydraulics systems; an advanced TPS covering, in particular, the nose and the leading edges of wing and tail.

In the present study, particular attention is focused on the vehicle TPS concept. From the Space Shuttle experience, the TPS has been identified as one of the area where large improvements can be made regarding operations and maintenance costs. Its mass fraction, equal to about 15% of the vehicle empty weight, is large enough to be targeted for potential mass saving. This mass saving, together with operational reentry trajectories, characterized by low inertial loads (i.e. vehicle with lightweight primary structures), lead to vehicles with low wing loading. Finally, with low wing loading and advanced aerodynamic configuration (e.g. high L/D) high performance vehicles can be attained.

The sharp leading edges can stand at hypersonic conditions if bulk self standing shapes Ultra High Temperature Ceramics (UHTC) are provided [6-7]. UHTC shapes spread out the region of high surface temperature over which radiative cooling is effective [8-10].

For the remaining vehicle parts, instead, Metal Matrix Composite (MMC), such as for example PM1000, are expected to be used. Practically, the TPS becomes very integrated with the vehicle "cold" structure.

This compares with, and differs from, the usual method of thermal protection that makes use of a leading edge, having significant radius of curvature (i.e. blunt bodies), made of refractory material such as, e.g., Reinforced Carbon-Carbon (RCC) as in the Space Shuttle case.

However, it is known that conduction-assisted radiative-cooling is an adequate thermal protection in reentry only if the heating rates are relatively low. This implies that the vehicle wing loading (W/S_r) must be kept small.

The above considerations, however, are by far for an exhaustive design approach for reentry vehicles.

The adopted concept is a conventional wing-body configuration with a sharp-leading-edges double-delta planform as basic shape. The configuration has a distinct wing body design with a blended wing body interface and a flat bottom surface to increase the overall hypersonic performance of the RTB. The three-view drawing of the vehicle are presented in Fig. 1

The forebody, instead, is characterized by a simple cone-sphere geometry with a sharp nose; while the overall vehicle length and the position of the wing are dictated by center of gravity (c.g.) position with respect to the aerodynamic center of pressure. In order to obtain satisfactory vehicle stability and controllability for major parts of the flight envelope the c.g. has to be close to vehicle centre of lift. So, the wing is placed near

the rear of the body and is also swept to assure best performance with respect to the supersonic drag and aerodynamic heating.

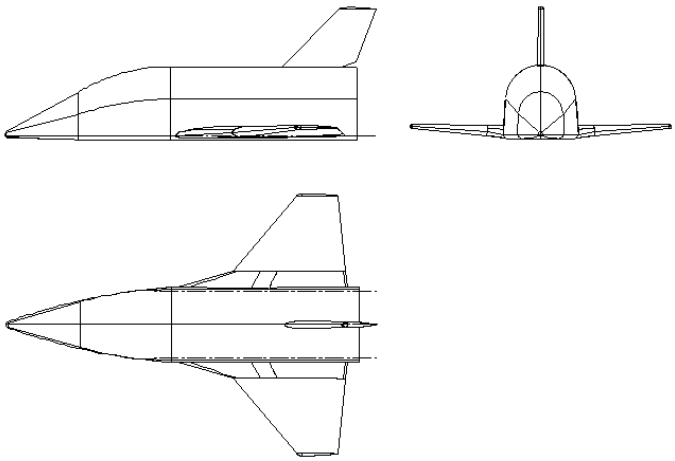

FIGURE 1 : Three View Drawing.

Furthermore, a dihedral angle is provided in order to enhance flight stability. The airfoil shape is maintained from root to wing tip and provides leading edge with small radius of curvature to reduce wave drag and to take advantage of the boundary layer thickening.

The control surface on the wings are elevons which must serve as ailerons, elevators, and flaps (due to heat buildup at the joints, split surfaces must be avoided). Therefore, the control surfaces deflect differentially and must be large enough to provide stability at landing speed, without sacrificing too much lift **Error! Reference source not found.**.

The vertical tail provides the vehicle sideslip stability. Note that along the low risk reentry the tail is effective unlike the classical reentry where, at high AoA, it is shielded from the flow providing no control [2].

In order to improve later on the vehicle aerodynamic and stability along the atmospheric descent, a body flap, extending from the base of the vehicle, is provided (at hypersonic speeds a surface behind the vehicle c.g. balances the nose up pitching moment provided by the vehicle forebody).

This additional control surface is also able to protect the engine nozzle, against aerodynamic heating when the spacecraft is flying at an AoA.

One of the most important inputs in the vehicle sizing process is the size requirement of the payload accommodation bay of the Expendable Launch Vehicle (ELV). In fact this requirement determines the overall dimensions of the demonstrator.

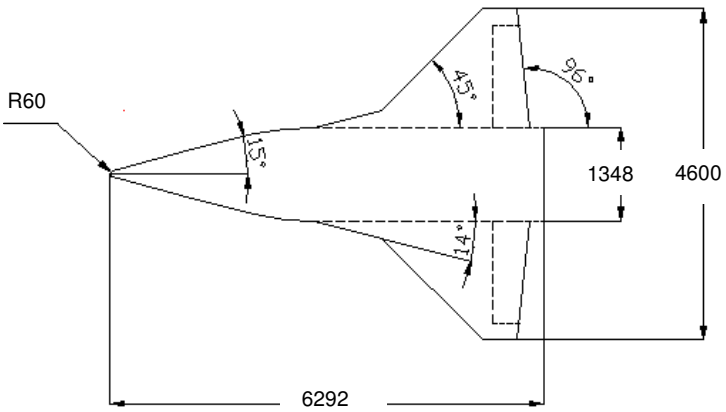

FIGURE 2 : RTB Dimensions, in [mm].

To take advantage of small low cost ELV, the following RTB dimensions (see Fig. 2) are used:

- total length (tail included) [m]: 6.400;
- fuselage length (L) [m]: 6.292;
- maximum fuselage width [m]: 1.348;
- wingspan [m]: 4.600;
- planform area [m^2]: 11.840;
- wing area (S_r) [m^2]: 9.344;
- nose radius (R_N) [m]: 0.060;
- wing leading edge radius (R_{WN}) [m]: 0.040.

The fineness ratio of the fuselage is approximately 5 while the wing aspect ratio is 2.26. A sweep angle of 45° provides a delta wing that does not extend far behind the fuselage and, in addition, minimizes the aeroheating on the sharp leading edge [12]. In order to increase stability, five degrees of dihedral angle is adopted. The vertical tail sweep angle is 45 degrees. The 3D Computer Aided Design (CAD) model of the vehicle is shown in Fig. 3.

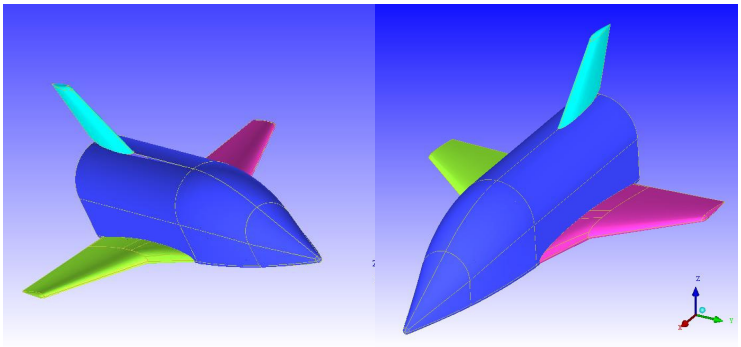

FIGURE 3 : The RTB CAD Image.

The following percentage data of the hypersonic flight demonstrator are provided (see Fig. 4):
- Structure: 25.0 %,
- Subsystems: 53.0 %,
- TPS: 16.0 %,
- Propellant: 6.0 %

keeping in mind that this vehicle represents a trade-off between a compact structure required to reduce reentry heating and a sleeker structure that can glide with an acceptable glide ratio and sink rate.

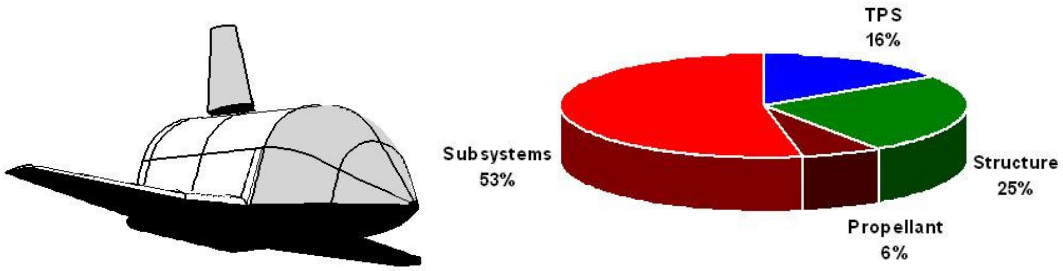

FIGURE 4 : Vehicle TPS Layout and Mass Budget.

3. REENTRY FLIGHT SCENARIO

CFD simulations of the flowfield past the RTB require several freestream conditions as for example Mach number, density, temperature, gas composition, and vehicle trim conditions (e.g. AoA and/or Angle of Sideslip - AoS). Those complete set of CFD input data are provided by the reentry flight scenario (e.g. at every point along the descent trajectory).

To this scope, the vehicle reentry flight scenario has been evaluated. A 6 degree-of-freedom (dof) model is used for describing the dynamics of the RTB and the vehicle performances have been determined by the complete trajectory simulations, from reentry to landing, as done by the code ENTRY developed in [13].

ENTRY performs the descent analysis once the complete data set of the vehicle aerodynamic coefficients, as function of the AoA, AoS, Reynolds number, and Mach number is provided.

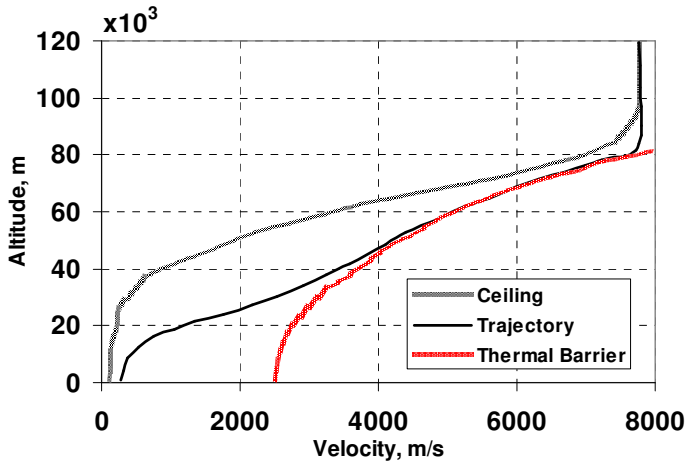

FIGURE 5 : Vehicle Reentry Scenario.

Fig. 5 shows the reentry design trajectory used to assess the vehicle aerothermodynamic environment for TPS design scopes; the reentry corridor is also shown. Time histories of reentry altitude and AoA are summarized in Fig.6.

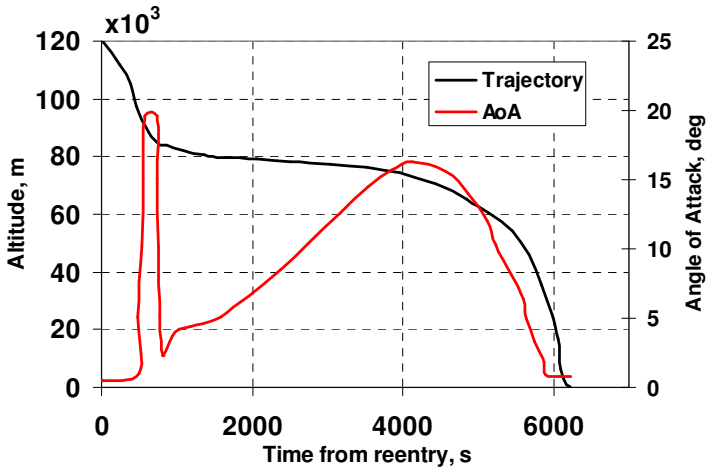

FIGURE 6 : Time History of Altitude and AoA.

As shown in Fig. 5 and Fig.6 , the reentry scenario envisages an enduring atmospheric gliding flight, during which the vehicle flies for a long period very close to the thermal barrier (e.g. the floor of reentry corridor). This extended-duration trajectory present a formidable challenge to TPS design due to the potential for large heat soaks into the airframe.

The vehicle, however, takes advantage of radiative equilibrium cooling i.e., the total aeroheating to the wall (both conductive and diffusive heating) is assumed to be equal to that re-radiated from the surface.

During the period of maximum aeroheating, as shown in Figs. 7 and 8, the vehicle Guide Navigation and Control (GNC) strategy is based on the AoA modulation. Therefore, the flight conditions at the AoA peak determines the freestream conditions to consider in the numerical computations of the vehicle aeroheating, as will be well explained hereinafter.

The aerothermodynamic environment of the airframe fuselage, nose, and leading edges have been calculated using again the ENTRY engineering code, as recognized in the next paragraph.

4. AEROHEATING ASSESSMENT

During reentry the RTB suddenly heats due to the dissipation, in the boundary layer, of its high energy (potential and kinetic) by friction with the atmosphere.

Knowing the freestream density, flight speed, nose and wing leading edge radii, and enthalpy variation with temperature, the stagnation point heat flux can be computed, thus providing a preliminary assessment of the vehicle aeroheating environment.

The simplest method for estimating hypersonic aerodynamic heating refers to the following general relationship [14], [15]:

$$\dot{q} = C\, \rho_{\infty}^{a}\, v_{\infty}^{b} \qquad (1)$$

where $\dot{q}$ is in [W/m^2], if the free-stream density ρ is given in [Kg/m^3], and the flight velocity v is given in [m/s].

With that formula one is able to describe the heat transfer at vehicle leading edges (i.e. nose, wing, and tail) and to flat bottom vehicle surfaces (i.e. fuselage and wing) if appropriate values for ***C***, ***a*** and ***b*** are provided. If:

$$\begin{cases} C = 1.83\text{x}10^{-4}\, \dfrac{1}{\sqrt{R_N}} \left(1 - \dfrac{h_w}{h_0}\right) \\ a = \dfrac{1}{2}, \quad b = 3 \end{cases} \qquad (2)$$

the stagnation point heat transfer at fuselage nose ($\dot{q}_N$) is described according to Ref. [15]; R_N is the nose radius in meters, $h_w = c_{pw} T_{rw}$ and $h_o = \dfrac{v_{\infty}^2}{2} + c_p T_{\infty} \cong \dfrac{v_{\infty}^2}{2}$ are the wall and total enthalpies, respectively [15].

In order to perform the vehicle windward surface heating analysis ($\dot{q}_{FP}$), if we consider the laminar flat plate case and the condition that $M_{\infty} \sin\phi > 1$, it follows that:

$$\begin{cases} C = 2.53\text{x}10^{-5}\, \dfrac{\sin\phi}{\sqrt{x}} \sqrt{\cos\phi} \left(1 - \dfrac{h_w}{h_o}\right) \\ a = \dfrac{1}{2}, \quad b = 3.2 \end{cases} \qquad (3)$$

where ϕ is the local body angle with respect to the free-stream (i.e. the local surface inclination plus the AoA), x is the distance, in meters, from the stagnation point measured along the body surface [14].

This last correlation formula highlights how it is preferable to have a vehicle windside flat surface because ϕ, in this case, is only the AoA.

To estimate the heat transfer at wing and tail ($\dot{q}_{LE}$) (i.e. vehicle swept leading edge) one can take advantage of both the above correlation formulas. In fact :

$$\dot{q}_{LE} = \sqrt{\left(\frac{1}{\sqrt{2}} \dot{q}_N \cos\Delta\right)^2 + \left(\dot{q}_{FP} \sin\Delta\right)^2}\, \cos\alpha \qquad (4)$$

where Δ is the leading edge sweep angle [14].

Naturally, the validity of this analysis is reasonable as long as flight conditions are such that the boundary layer theory is valid. Note that if we let the characteristic length be a running distance x from the nose or leading edge of the vehicle, then the Knudsen number becomes infinite when x=0 (Kn=λ/x, where λ is the mean free molecular path). To address the effects of rarefaction on the nose heating calculation, the free molecules (fm) heating rate ($\dot{q}_{fm}$) is estimated by Eq. (1) with:

$$\begin{cases} C = \dfrac{St_o}{2}\left(1 - \dfrac{h_w}{h_o}\right) \\ a = 1, \quad b = 3 \end{cases} \tag{5}$$

The Stanton number at the stagnation point (St_o) is a function of the Cheng and Chang rarefaction parameter (K_r^2), that is close to the Reynolds number behind the bow shock wave [16]. In Ref [16] it is shown that K_r^2, in the range of interest, leads to $\dot{q}_{fm} > \dot{q}$. So the continuum formulas, Eq. (1) and Eq. (4), are conservative.

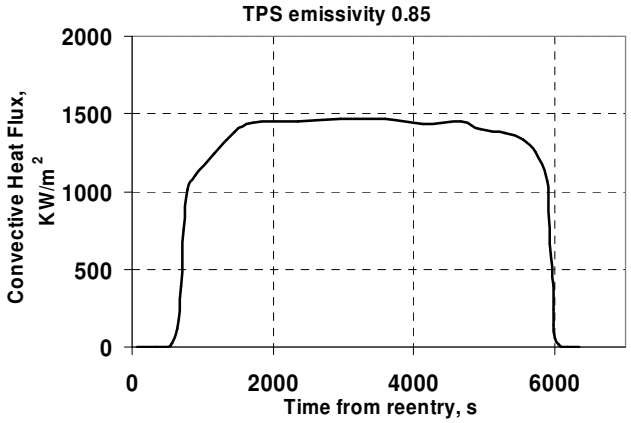

FIGURE 7 : Heat Flux Profile During Reentry.

The vehicle aerothermal environment as predicted by Eq. (1) is summarized in Fig. 7, where the convective heat flux, with the wall in radiative equilibrium condition, is reported for the vehicle nose.

The time history of the corresponding radiative equilibrium temperature can be recognized in Fig.8, supposing that the TPS emissivity is equal to 0.85.

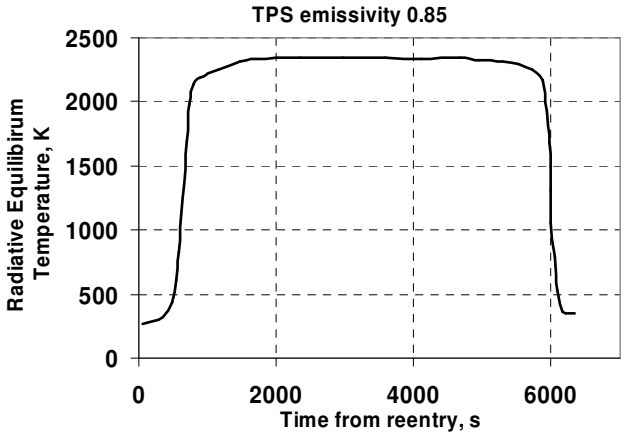

FIGURE 8 : Radiative Equilibrium Temperature.

This overall analysis appears to be conservative if one takes into account the effect of material thermal conductivity of the TPS [17].

However, the heat flux profile is only one criterion in the design of the TPS. For example, also the pressure is important since it determines the TPS structural strength, to maintain the vehicle aerodynamic shape [18]. The other important criterion to consider is the area under the heat flux curve (i.e. the integrated heating rate over the time allotted by the descent trajectory). This area is also referred to as integrated heat load (IHL):

$$Q(\vec{r}) = \int_{t_i}^{t_f} \dot{q}(\vec{r}, t)\, dt \qquad (6)$$

In fact, while the peak heat flux guides the selection of Thermal Protection Material (TPM) able to withstand the heat flux peak, the IHL determines the thickness of the TPM (i.e. the TPS thickness determines the thermal budget that the structure has to manage to protect the "cold" vehicle structure). Therefore, in the framework of TPS vehicle design, one should select on the vehicle reentry trajectory, a number of points for computational analysis (control points), able to replicate the area under the heat pulse. The leftmost point (early on the trajectory) on the heat pulse is chosen from continuum considerations, (i.e., the Knudsen number based on the vehicle characteristic dimension does not exceed 0.001 and the convective heat flux has a "reasonable value"). On the contrary the rightmost point on the heat pulse is chosen from either a desired dynamic pressure, or Mach number limit (e.g., $M_\infty \leq 4$), while the other points are distributed between these two. These engineering evaluations, however, are not sufficient to guarantee a reliable estimation of the vehicle aeroheating. More accurate computation is needed by using CFD analyses, as done in the next paragraph.

4.1 Aerothermal Analysis by CFD

As far as the heat flux distribution over the vehicle surface is concerned, a trajectory check point (freestream conditions at the flight point) has been considered, in the framework of a trajectory-based design approach. This point, shown in Fig.9, represents the most challenging flight conditions from the aeroheating point of view, since the vehicle is flying along the thermal barrier at the higher AoA (see Fig.5 and Fig.6). The freestream conditions are $Mach_\infty$=22.4, H_∞=73.1 [Km], and AoA=16.5 [deg], as given in Table 1.

TABLE 1 : Freestream Conditions for CFD Analysis.

Altitude [km]	Pressure [Pa]	Temperature [K]	Density [Kg/m^3]	Mach [-]	AoA [deg]
73.1	3.28	212.3	5.38×10^{-5}	22.4	16.5

4.1.1 Heat flux modeling

The aeroheating analysis of a vehicle reentering from space demands different physical approach to implement in the numerical simulations. In fact, as recognized in Fig. 5 and Fig. 9, the vehicle experiences different flight regimes ranging from free molecular flow at very high altitudes to complete continuum deep in the atmosphere. Most of the heating occurs, however, in the continuum regime, where the CFD approach, based on the integration of the Navier-Stokes equations (with appropriate physical models for shock layer processes), is adequate [19].

Generally speaking the air is modeled as a mixture of several species (up to 11 species), each one assumed to be thermally perfect, and the main requirements for the models are: *thermodynamic* and *transport* (mass, momentum, and energy) properties of the constituent species; accurate representation of reactions (e.g. *reaction mechanism*), and their associated rates (e.g. *chemical kinetics*) in the shock layer; the models for *thermal nonequilibrium*, if necessary, as in the case of substantial radiative heating.

A rough estimation of how many chemical species to consider in the numerical computation may be found analyzing the post-shock species distributions provided by a simple one-dimensional equilibrium computation for a normal shock corresponding to the freestream conditions at the trajectory points.

Moreover, there are three important modeling issues that need further attention within aeroheating analysis: *gas-surface interaction*, *transition*, and *turbulence* [20].

At the vehicle surface, apart from the usual "no-slip" and zero normal pressure gradient boundary conditions at the wall, mass and energy balance equations are necessary to represent the interaction of the gas and surface (e.g. heterogeneous reactions).

The mass balance equations are obtained considering that the flux due to mass diffusion is balanced by the production of molecular species through recombination of atoms:

$$\vec{J}_{s_w} \cdot \hat{n}_w = \rho_{s_w} \gamma_{s_w} (T_w) \sqrt{\frac{\Re T_w}{2\pi M_s}} \qquad (7)$$

When γ_s=1, the wall permits complete recombination of atoms at the surface (e.g. Fully Catalytic Wall – FCW). If γ_s=0, the surface does not permit recombination and it is said to be noncatalytic (NCW). The heat released due to recombination at wall is maximum for FCW, and zero for NCW. However, for a real TPM, the recombination coefficient is between the two extremes, i.e., $0 \le \gamma_s \le 1$ and is a characteristic of the material.

Further, recombination coefficients are functions of temperature, i.e., $\gamma_s = \gamma_s(T)$. As preliminary TPS design criteria, the conservative assumption of a FCW is preferred since one can expect maximal heat release from recombination. Note that in the case of air, the surface is assumed to be noncatalytic to NO and permits only recombination of N and O. Secondly, radiative equilibrium is assumed to exist at the wall.

Therefore, the energy balance equation at the surface, neglecting in-depth conduction through the TPS, reads:

$$-k_w \vec{\nabla} T \cdot \hat{n}_w + \sum_{s=1}^{n_s} h_s (T_w) \vec{J}_{s_w} \cdot \hat{n}_w = \sigma \varepsilon_w T_w^4 \qquad (8)$$

where the emissivity, in general, depends on the temperature and the type of TPM, i.e., $\varepsilon_w = \varepsilon_w(T_w, \text{TPM})$.

The other important issues that affect the convective heating at the wall are transition and turbulence. Since the onset of transition cannot be predicted *a priori*, the results from laminar computations are post-processed for boundary-layer momentum thickness and edge Mach number. The ratio of the momentum thickness Reynolds number to the edge Mach number is used as a guide to determine the onset of transition empirically through correlation of computed laminar boundary-layer parameters (notably the momentum thickness) with experimental data. Note that this is only one of many criteria, and assumes the body is smooth. Irregularities in the surface — either roughness or steps/gaps — could cause transition to occur earlier.

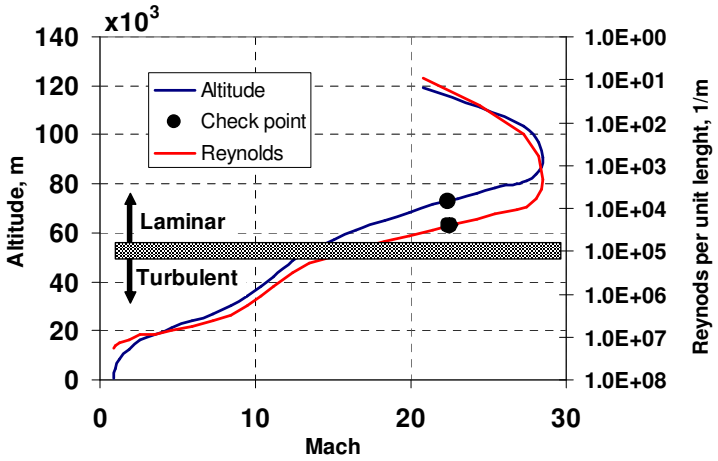

FIGURE 9 : Reentry trajectory in Altitude – Mach and unit Reynolds-Mach planes.

Assuming that onset of transition can be determined using the momentum thickness Reynolds number criterion, the length of the transition region must be predicted. For the lack of a good transition model, the assumption of a fully turbulent flow is usually made, and an algebraic turbulence model is used, e.g., the Baldwin Lomax model corrected for compressibility — reasonably good for attached flows but not so for separated leeside flows. Such an assumption can be excessively conservative in the design of the TPS — simply due to predicted high levels of heating in forward part of the configuration.

The shaded region in Fig. 9 refers to unit Reynolds number equal to 10^5 above which the flow is assumed fully turbulent. Thus, a selected flight condition lying under this boundary (see Fig. 9) requires a turbulent flow computation. It is worth nothing that the unit Reynolds number, during the critical aeroheating phase of atmospheric descent, is less than the threshold value, i.e. it is above the dashed region of Fig. 9. Therefore, for the computations reported in this work the issues of transition and turbulence are neglected.

4.1.2 Grid generation

In the framework of the flow field computational analysis a relevant issue is to build an accurate volume mesh. The multiblock mesh on the vehicle surface is shown in Fig.10.

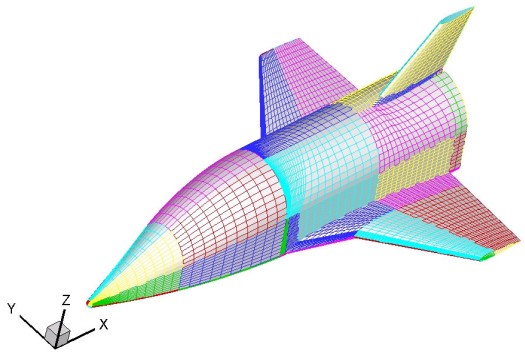

FIGURE 10 : Multiblock Mesh on the Vehicle Surface.

Since no sideslip flow has been taken into account, the grid has been built only over either the port or starboard half of the vehicle. The distribution of surface grid points is dictated by the level of resolution required in various areas, e.g., the bow shock-wing shock interaction region for a winged vehicle requires fine resolution. The distribution of grid points in the wall-normal direction are driven by the freestream Reynolds number in order to require adequate spacing to resolve the thin shear layer bound to the wall. The grid is then tailored for the freestream conditions at the selected trajectory point (see Table 1).

4.1.3. CFD results

CFD analyses of the vehicle along the descent flight path are needed to confirm (and/or to correct) the results of the engineering approach followed above; and to assess that, during reentry, the radiative equilibrium temperature distribution of the skin of the remaining vehicle structure (fuselage and wing), made of conventional material, be below the tolerable limits (i.e. about 1500 [K] for the PM1000).

The flow conditions considered for the numerical simulations are summarized in Table 1. Computation is performed at (conservative) steady state conditions and solves the flowfield using a local radiative equilibrium wall-boundary condition. Moreover, simulations are performed at laminar flow conditions with the flow modeled as perfect gas with constant specific heat, thermal conductivity described by kinetic theory and viscosity derived from Sutherland law; these assumptions are acceptable since the air can be assumed as “frozen” gas mixture because of the streamlined vehicle configuration. Numerical computations show that the flowfield is dominated, in fact, by the presence of a weak bow shock wave, as shown in Fig.11.

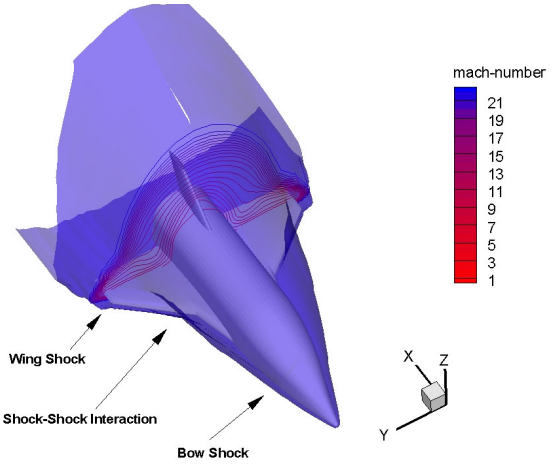

FIGURE 11 : Shock Shape with Mach Number Contours.

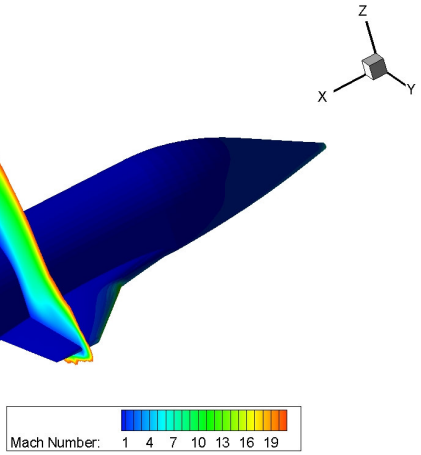

FIGURE 12 : Mach Number Contours in the Vehicle Cross-Section at x=5.5 [m].

Looking at Fig.11 and Fig.12 one can appreciate the shock shape that occurs ahead of vehicle at this flight conditions, with the Mach number contour field on the vehicle cross section at x=5.5 m (see Fig.12). As one can see, the shock surface envelopes the vehicle, and since the vehicle features a small radius of curvature, the stand-off distance is quite small. Therefore, the bow shock may impinge on wing leading edge and vertical fin thus increasing locally the heat flux (overheating) that the vehicle thermal shield has to withstand.

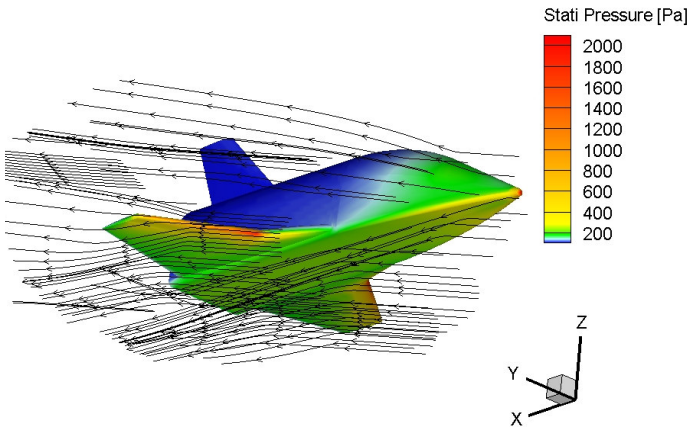

FIGURE 13 : Flow-field Streamlines with Static Pressure Contours on the Vehicle.

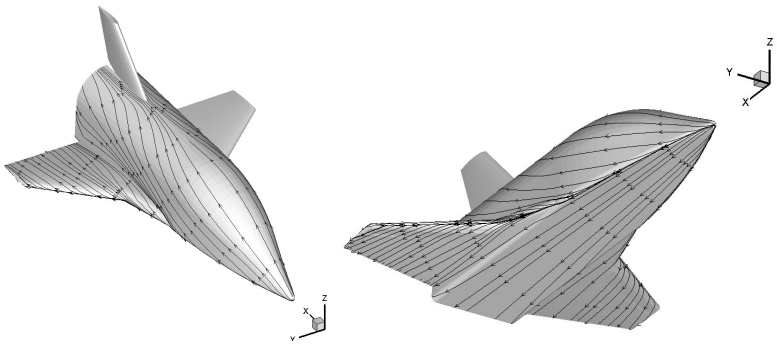

FIGURE 14 : Vehicle Skin Friction Patterns.

The flow-field streamlines around the vehicle can be recognized in Fig.13, where the pressure distribution on the vehicle surface is also reported. In Fig.14 it is shown the surface streamlines distribution on the whole

vehicle configuration. As one can see on the fuselage forebody and strake, 3D effects are present as highlighted by the curvature of the lines at the wall, whereas the wing part between the tip and the strake experiences a quasi 2D flowfield.

The three-dimensional distributions of pressure and heating on the vehicle were evaluated to establish TPS design guidelines. For example, both Fig.15 and Fig.16 report the static pressure distributions on the vehicle surface. In particular, Fig.16 shows the detail of pressure distribution on wing leading edge, thus highlighting the effects (e.g. pressure spike) of the bow shock impingement (known as Shock-Shock Interaction) on Wing Leading Edge (WLE), (see also Fig.11).

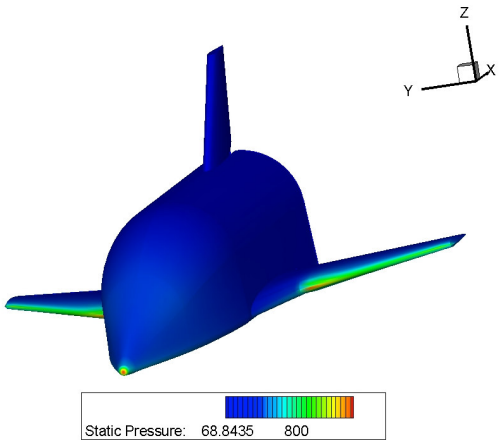

FIGURE 15 : Contours of Static Pressure [Pa].

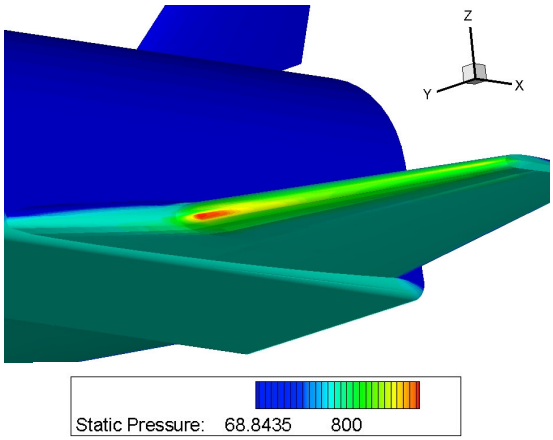

FIGURE 16 : Contours of Static Pressure [Pa]; Detail on the Wing Leading Edge.

Figure 17, Fig. 18 and Fig. 19 show the surface distribution of the radiative equilibrium temperature. The TPS emissivity is supposed equal to 0.85. These distributions highlight that, on the spacecraft, the aeroheating is comparable with that of windward. Therefore, it would be reasonable to design the leeward TPS distribution similar to that of windside.

As a result, careful attention has to be made in defining the vehicle TPS layout. In fact, for the conventional reentry vehicle such as the Space Shuttle, the peak heating conditions occur when the spacecraft is flying at 40 deg of AoA, thus exposing to the oncoming flow only the windward side that is the most heated vehicle part. It is worth to note that, as shown in Fig.17, the CFD confirms the results provided by Eq.(1) for the vehicle stagnation region.

Then, candidate TPS materials may be selected to accommodate the maximum radiation equilibrium temperatures shown in Fig. 17, Fig. 18 and Fig. 19, taking into account that: the actual surface temperatures

of the vehicle will be lower than these radiation equilibrium temperatures because of heat-sink effects of the structure; and transient thermal analyses is mandatory in order to determine TPS thickness of the vehicle thermal shield.

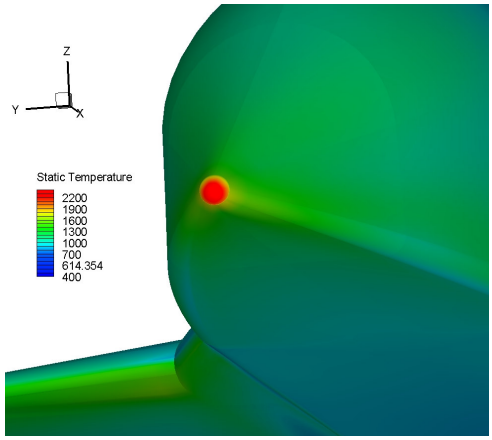

FIGURE 17 : Contours of Radiative Equilibrium Temperature [K]; Detail of the Nose Region.

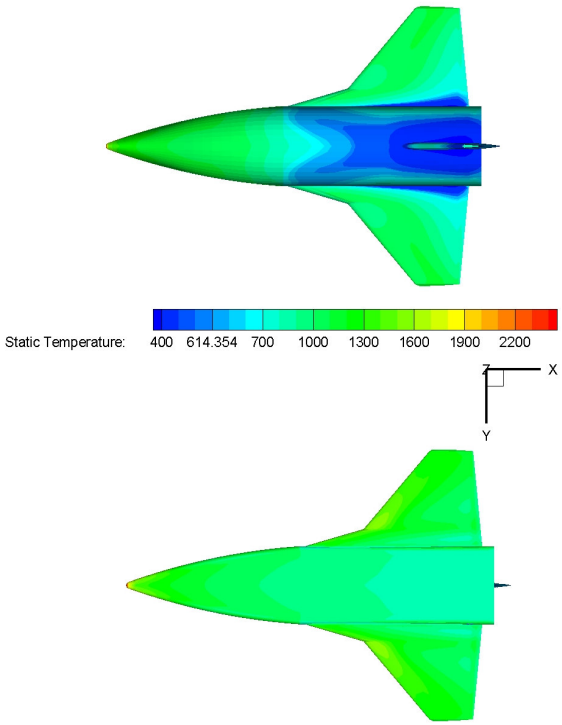

FIGURE 18 : Contours of Radiative Equilibrium Temperature [K] on the Leeside (up) and Windside of the Vehicle (down).

Moreover, it can be concluded that an analysis of SSI with overloads (pressure and heat flux) at impingement are mandatory for a reliable vehicle TPS layout as vehicle design proceeds, since difference on heat flux distribution are expected moving in span wise direction toward the tip (see Fig. 19). Indeed, the part of the wing that is behind the vehicle bow shock experiences different flowfield conditions with respect to the freestream ones: the most heated zone of the wing is the one inside the bow shock.

Note that the position of the high heat load region localized on the WLE by SSI changes along the atmospheric descent, depending on Altitude, Mach and AoA reentry profiles (i.e. it varies from point to point along the trajectory). Moving along the leading edge, in the span wise direction, there is a quite constant temperature value due to the constant leading edge radius.

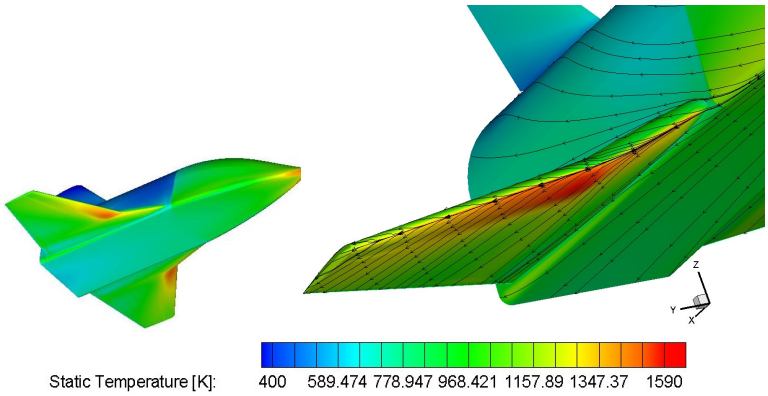

FIGURE 19 : Contours of Radiative Equilibrium Temperature [K] with Skin Friction Lines; Detail on the Wing Leading Edge.

A developmental TPM concepts, known as Ultra High Temperature Ceramics (UHTC) were identified that seems to offer significant advantages in thermal shielding capability when the temperature involved are in exceed of 1700 [K] [20]. UHTC, in fact, are able to withstand to temperature up to 3000 [K] as the HfB_2 (Hafnium diboride). Therefore they are very promising for the operability of the future hypersonic vehicles and represent an enabling technology for next generation RLVs. These TPM concepts are being developed by the NASA Ames Research Center as part of the "next generation reusable TPS" effort [6], [20]. An advanced metallic TPS concept with structure fabricated from Inconel alloy honeycombs was also considered for the vehicle surfaces away from leading edges.

Finally, in Fig. 20 and Fig. 21 it is shown the bow shock shape in a xy plane passing through the vehicle WLE. One can clearly appreciated where the SSI takes place on the WLE.

Note how the bow shock is close to the vehicle forebody due to its slender configuration. This confirms that the real gas effects are expected to be negligible compared with those take place for bluff body configuration such as that of Space Shuttle.

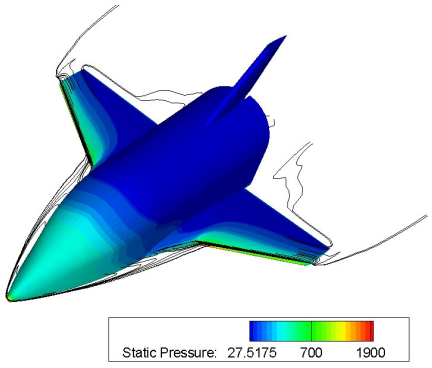

Figure 20 : Contours of Static Pressure [Pa] with Shock Shape Trace in a xy Plane Passing through the Vehicle WLE.

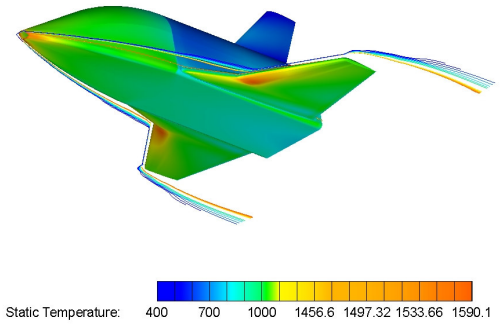

FIGURE 21 : Contours of Radiative Equilibrium Temperature [K] with Shock Shape Trace in a xy Plane Passing through the Vehicle WLE.

5. CONCLUSIONS

The aero-thermal environment of a TSTO flying test bed has been assessed both from the engineering based and CFD based approaches. Computations with the air modelled as perfect gas highlight that the vehicle aeroheating is more severe than that of existing reentry vehicles, since the RTB features a streamlined configuration and flies at low angle of attack in order to improve spacecraft aerodynamics.

Also, new technologies for RLV, for which strong necessity of in-flight testing exists, were identified. Although there are many mature TPS materials, only advanced thermal shield using TPM such as UHTC, being developed, will be able to withstand the radiative equilibrium temperatures reached during reentry. A major task of this work has been the study of vehicle concepts and related enabling technologies required for the goal of a highly safe return to Earth.

Finally, we observe that the RTB provides a completely novel approach to the reentry problem. It has some very attractive features, although some are yet unproven, that are mostly derived from its low wing loading. There appears a strong case for continuing the current project study: the development of a European reusable launch vehicle, for which hypersonic flight demonstration is an indispensable next step.

6. REFERENCES

[1] Dumbacher D., *"NASA's Second Generation Reusable Launch Vehicle Program Introduction, Status and Future Plans"*. 38th AIAA/ASME/SAE/ASEE Joint Propulsion Conference and Exhibit, Indianapolis, Indiana, July 7-10, 2002. AIAA-2002-3613.

[2] Whitmore S., Dunbar B., *"Orbital Space Plane, Past, Present, and Future"*. AIAA International Air and Space Symposium: The Next 100 Years, Dayton, Ohio, July 14-17, 2003. AIAA-2003-2718

[3] Rasky D., *"Access from Space: A New Perspective on NASA's Space Transportation Technology Requirements and Opportunities"*. Space 2004 Conference, San Diego, California, Sep. 28-30, 2004. AIAA-2004-6103.

[4] Reuther, J., Kinney, D., Smith, S., Kontinos, D., Gage, P., Saunders, D., *"A Reusable Space Vehicle Design Study Exploring Sharp Leading Edges"*. AIAA Thermophysics Conference, 35th, Anaheim, CA, June 11-14, 2001. AIAA-2001-2884.

[5] Saunders, D., Allen, G. Jr., Gage, P., Reuther, J., *"Crew Transfer Vehicle Trajectory Optimization"*. 35th AIAA Thermophysics Conference, Anaheim, CA, June 11-14, 2001. AIAA-2001-2885.

[6] Kolodziej, P., Bowles, J. V., Roberts, C., *"Optimizing Hypersonic Sharp Body Concepts from a Thermal Protection System Perspective"*. 8th AIAA International Space Planes and Hypersonic Systems and Technologies Conference, Norfolk, VA, Apr. 27-30, 1998, paper AIAA-1998-1610.

[7] Chen, Y. K., Milos, F. S., Bull, J. D., Squire, T. H., *"Integrated analysis tool for ultra-high temperature ceramic slender-body reentry vehicles"*. 37th Aerospace Sciences Meeting, Reno, NV, Jan. 11-14, 1999. AIAA-1999-350.

[8] Kontinos D. A., Gee K., Prabbu D. K., *"Temperature constraints at the sharp leading edge of a Crew Transfer Vehicle"*. 35th AIAA Thermophysics Conference, Anaheim, CA, June 11-14, 2001.

[9] Lee C. H., Park S. O., *"Aerothermal performance constraints for small radius nosetip at high altitude"*. AIAA/NAL-NASDA-ISAS 10th International Space Planes and Hypersonic Systems and Technologies Conference, Kyoto, Japan, Apr. 24-27, 2001. AIAA-2001-1823.

[10] Jeroen Buursink, Kees Sudmeijer, *"Experimental Studies of an Enhanced Radiation Cooling System".* Space 2004 Conference and Exhibit, San Diego, California, Sep. 28-30, 2004. AIAA-2004-5827.
[11] Smith S., Reuther J., Kinney D., Saunders D., *"Low speed aerodynamics and landing characteristics of Sharp-class Crew Transfer Vehicle concepts".* 35th AIAA Thermophysics Conference, Anaheim, CA, June 11-14, 2001.paper AIAA-2001-2888.
[12] Gomg L., Ko W.L., Quinn R.D., "*Thermal Response of Space Shuttle Wing During Reentry Heating".* NASA TM 85907, June 1984.
[13] Viviani A., Pezzella G., Cinquegrana D., *"Aerothermodynamic Analysis of an Apollo-like Reentry Vehicle"*. AIAA-2006-8082.
[14] Tauber E., *"A review of High-Speed, Convective, Heat-Transfer Computation Methods".* NASA TP-2914, Jul 1989.
[15] Anderson J. D., *"Hypersonic and High Temperature Gas Dynamics".* McGraw-Hill (series in Aeronautical and Aerospace Engineering), 1989.
[16] Cheng H.K., Chang A.L. *"Stagnation Region in Rarefied High Mach Number Flow*". AIAA J.,1(1),1963.
[17] Loomis M., Palmer G., *"Pre-flight CFD analysis of arc jet and flight environments for the SHARP-B2 flight experiment".* 39th Aerospace Sciences Meeting, Reno, NV, Jan. 8-11, 2001. AIAA-2001-982.
[18] Kinney, D. J., Bowles, J. V., Yang, L. H., Roberts, C. D., *"Conceptual design of a SHARP–CTV".* AIAA Thermophysics Conference, 35th, Anaheim, CA, June 11-14, 2001. AIAA-2001-2887.
[19] Zuniga F., Cliff S., Kinney D., Hawke V., Tang C., Smith S., *"Vehicle Design of a Sharp CTV Concept Using a Virtual Flight Rapid Integration Test Environment".* AIAA Atmospheric Flight Mechanics Conference and Exhibit, Monterey, California, Aug. 5-8, 2002.AIAA-2002-4881.
[20] Johnson S., Gasch M., Leiser D., Stewart D., Stackpool M., Thornton J., Espinoza C*., "Development of New TPS at NASA Ames RC".* 15th AIAA International Space Planes and Hypersonic Systems and Technologies Conference, Dayton, Ohio, Apr. 28-1, 2008. AIAA-2008-2560.